Polarisation Analysis of in-situ observations of Langmuir/Z-mode waves by Solar Orbiter

T. Formánek[1,2], O. Santolík[2,3], J. Souček[2], D. Píša[2], A. Zaslavsky[1], M. Maksimovic[1], M. Kretzschmar[4], C. J. Owen[5], J. Rodríguez-Pacheco[6]

[1]LIRA, Observatoire de Paris, Université PSL, CNRS, Sorbonne Université, Université Paris-Cité, France
[2]Czech Acadademy of Sciences, Institute of Atmospheric Physics, Dep. of Space Physics, Prague, Czechia
[3]Faculty of Mathematics and Physics, Charles University, Prague, Czechia
[4]LPC2E, OSUC, CNRS/University of Orléans/CNES, Orléans, France
[5]Mullard Space Science Laboratory, University College London, UK
[6]Space Research Group, Universidad de Alcalá, Alcalá de Henares, Madrid, Spain

Tomas.Formanek@obspm.fr

Introduction

- Type III radio bursts are triggered by solar energetic events releasing electron beams into the solar wind.
- These beams create an unstable electron velocity distribution, generating Langmuir waves along its way to restore a single-peaked velocity distribution.
- Langmuir waves are usually electrostatic and linearly polarised along the magnetic field, but some observations show transverse electric fields.
- Langmuir/Z-mode waves serve as a generalisation of Langmuir waves for oblique propagation and exhibit transverse fields.
- We perform the first polarisation analysis of the Langmuir/Z-mode waves including its magnetic component.
- Our approach: compare numerical dispersion solutions with in-situ wave observations.

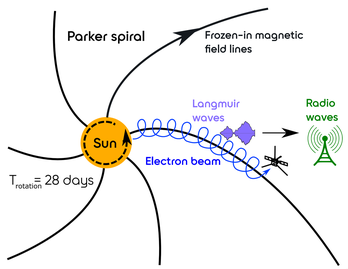

Figure 1: Representation of how a type III radio emission is produced in the solar wind.

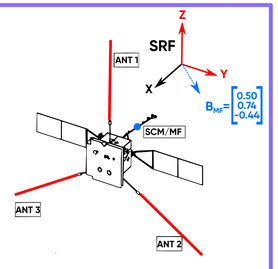

Figure 2: Representation of the orientation of electric antennas and search coil magnetometer in the spacecraft reference frame (SRF).

In-situ observations

Event overview:
Date: October 22, 2022 **Heliospheric distance: 0.5 AU**

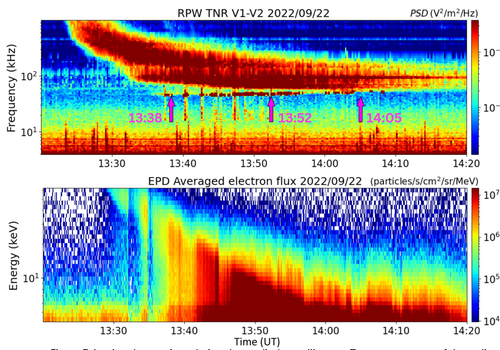

Figure 3: In-situ observations during the studied type III event. Top: spectrogram of the radio emission and Langmuir waves, highlighting the three studied timestamps. Bottom: measurement of the electron beam by the EPD SupraThermal Energetic Particles (STEP) sensor.

Instruments:
Radio and Plasma Waves (RPW) - Electric and Magnetic waveform data
Energetic Particle Detector (EPD) & Solar Wind Analyser (SWA) - electron velocity distribution function (VDF) data

Methodology:

Electron VDF fitting
- Fitted the observations from 13:38 UT and 14:05 UT using 8 **Maxwellians**
- Parameters: density, temperature, parallel velocity, anisotropy
- Poisson distribution maximum likelyhood method:

$$P = \prod_i p(N_i) \quad p(N_i) = \frac{e^{-n_i} n_i^{N_i}}{N_i!}$$

N_i - observations, n_i - model

Wave observations
- The waveform measurements at 13:52 UT show the strongest electric fields during the type III event.
- The Magnetic field signal from the Search Coil Magnetometer (SCM) exceeds the noise threshold.
- Coherent signal at the plasma frequency allows to study the observed polarisation.
- Determination of relative phases and amplitudes of observed components

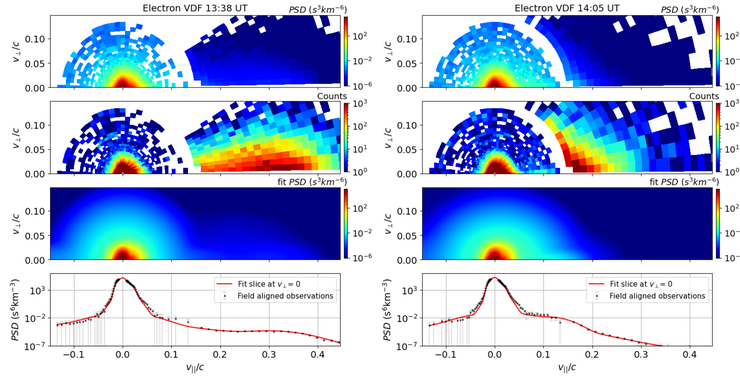

Figure 4: Observations and model of the electron VDF. The first row shows the phase space denisty observed by SWA and EPD. The second row shows the raw observed counts. The third row displays the fitted model of the VDF and the last row shows a slice along parallel velocities, comparing the model and observations.

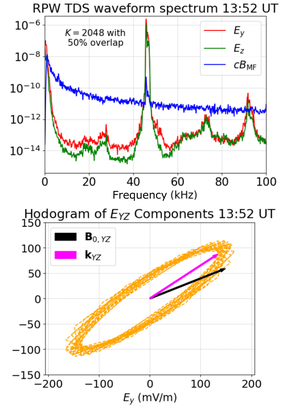

Figure 5: Top: spectrum of the waveform recorded during the middle timestamp of 13:52 UT. Bottom: hodogram of the peak amplitudes within the waveform observed at 13:52 UT with the direction of the background **B** field (black) and predicted wave vector direction (purple).

Solution of the dispersion relation

We solve the dispersion relation using code based on WHAMP for the timestamps of 13:38 & 14:05 UT
(Roennmark, 1982; Santolík et al., 2010)

Time averaging of observations
-> Fast evolving features are smeared out
EPD STEP: 60s (1s cadence), SWA EAS: 600s (10s cadence)

VDF stability and growth rates
- Both fitted VDFs are marginally stable
- At 13:38 UT, beam resonance at oblique angle
- Observed plateau at 14:05 UT -> low damping
- Distribution meets Gardner's stability condition *(Gardner, 1963)*

x Waves observed throughout the studied period

Oblique wave growth
- Weak beam population in part due to averaging -> study the results of modifying the beam
- Modification of the beam parallel temperature results in positive growth rate - its peak remains at at oblique wave vectors. Similar results for increasing beam density.
- A plateau population is causing the shift from parallel wave vectors
-> Parallel growth rate without the plateau

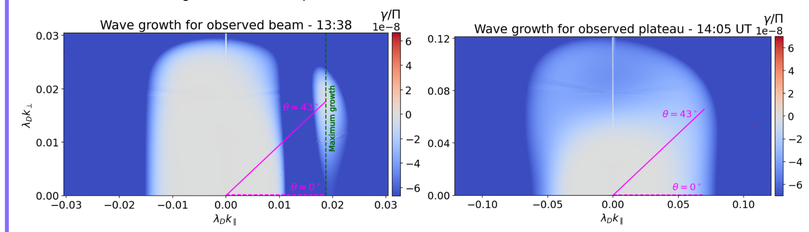

Figure 6: Wave growth obtained from WHAMP for the observed distributions at 13:38 and 14:05 UT. The purple lines highlight wave vector angles - the 43° angle corresponds to the maximum growth rate at 13:38 UT. The green dashed line corresponds to the Landau resonant $k_\parallel$.

Prediction of the polarisation
- Finding eigenfunctions of the dispersion matrix:

$$\mathcal{D} \cdot \mathbf{E} = 0$$

-> Dispersion relation and components of E, B
-> Project the fields onto directions observed by RPW
- We obtain a **prediction** of the observed relative phases and amplitudes (->polarisation)

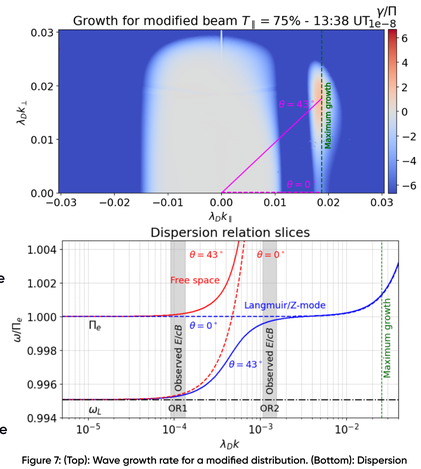

Figure 7: (Top): Wave growth rate for a modified distribution. (Bottom): Dispersion relation of the Langmuir/Z-mode and the free space L-O mode with wavevectors parallel (dashed lines) and at θ=43° (full lines). Regions highlighted in gray correspond to the observed ratio of the E/cB fields.

Observed wave polarisation

Observed polarisation
- Waveform split into 2048 sample segments -> Fourier transform
- Polarisation information hidden within the components of the spectral matrix:

$$\mathbf{S} = \begin{bmatrix} \langle E_Y E_Y^* \rangle & \langle E_Y E_Z^* \rangle & \langle E_Y B_{MF}^* \rangle \\ \langle E_Z E_Y^* \rangle & \langle E_Z E_Z^* \rangle & \langle E_Z B_{MF}^* \rangle \\ \langle B_{MF} E_Y^* \rangle & \langle B_{MF} E_Z^* \rangle & \langle B_{MF} B_{MF}^* \rangle \end{bmatrix}$$

Observed values:
$\Delta\Phi_{YZ}$ = (-12±5)°
$\Delta\Phi_{YB}$ = (-91±5)°
$\Delta\Phi_{ZB}$ = (-80±5)°
$E^2/(cB)^2$ = (6±2)10³

- Relative phases and amplitude ratio of E/cB shown in Figure 8
-> Compare with WHAMP

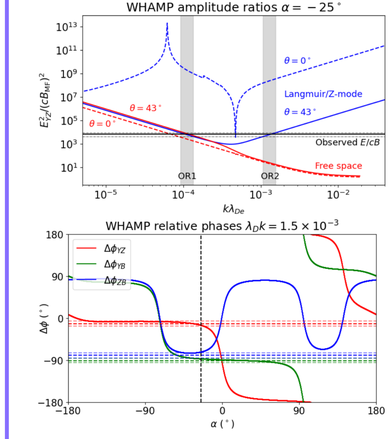

Figure 9: Comparison of wave polarisation parameters. Top panel compares the E/cB amplitude ratio. Bottom panel compares the relative phases between components.

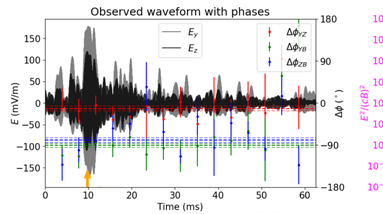

Figure 8: Waveform measurements from 13:52 UT showing the waveform and relative phases (left) and the E/cB amplitude ratio and signal coherence of the same waveform snapshot (right).

Comparison with WHAMP
- Finding a match between the observed value of relative phases and amplitudes
- Free parameters: wave vector size, angle θ between **k** and $\mathbf{B}_0$, azimuthal angle α of k - (due to gyrotropy)

-> Observed E/cB ratio requires a smaller k compared to the beam resonant region from Figures 6 and 7
-> Two regions with a matching amplitude ratio highlighted in Figure 9
- Change of α affects the projection and thus also E/cB.

- OR1 Relative phases do not match for any given azimuthal angle
- OR2 We find a match for all 3 relative phases and the E/cB ratio between WHAMP and observation

k-shifting mechanisms discussed in Malaspina et al., (2011)

Getting to oblique angles
- Wave growth at oblique angles + propagation into higher density
- Wave growth at parallel k + refraction on density gradients
- Electrostatic decay - nonlinear interaction: L -> L' + S

Conclusion

We analysed the polarisation of the first **coherent** observations of the **magnetic component** of a **Langmuir/Z-mode**. The electron VDF observations allowed us to compare the polarisation of the observed waves to a theoretical prediction based on the **numerical solution of the dispersion relation.** The comparison of the wave observations at 13:52 UT with the solution of the dispersion relation from neighbouring timestamps, revealed that the observed wave polarisation matches the Langmuir/Z-mode branch with a **lower wavevector magnitude** than where the wave would **grow due to Landau resonance.** Matching the relative phases and amplitudes of the observations and the WHAMP solution allowed us to determine the wavevector amplitude and direction. Several mechanisms for the generation of such low **k** transverse waves could be responsible.

Acknowledgements

This work was supported by state funding under the France 2030 program, managed by the French National Research Agency (ANR), reference ANR-23-CMAS0041.

Outstanding Student & PhD candidate Presentation contest

Sharing not permitted